Coupling of a Growth Kinetic Model of Gas Hydrate Formation With Gas-(Water-in-Oil) Slug Flow

Carlos Lange-Bassani, Fausto A. A. Barbuto, Vinicius R. de Almeida, Jean-Michel Herri, Amadeu K. Sum, Ana Cameirão, Rigoberto E.M. Morales

Coupling of a Growth Kinetic Model of Gas Hydrate Formation With Gas-(Water-in-Oil) Slug Flow

C.L. Bassani[1,2], F.A.A. Barbuto[1], Vinicius R. de Almeida[2], J.M. Herri[2], A.K. Sum[3], A. Cameirão[2] and R.E.M. Morales[1*]

[1]Multiphase Flow Research Center (NUEM), Federal University of Technology – Paraná (UTFPR), Rua Deputado Heitor Alencar Furtado, 5000, Bloco N, CEP 81280-340, Curitiba/PR, Brazil

[2]Mines Saint-Etienne, Univ Lyon, CNRS, UMR 5307 LGF, Centre SPIN, Departement PEG, F - 42023 Saint-Etienne France

[3]Hydrates Energy Innovation Laboratory, Chemical and Biological Engineering Department, Colorado School of Mines, 1500 Illinois St., Golden, CO 80401, USA

asum@mines.edu, cameirao@emse.fr, rmorales@utfpr.edu.br

Keywords: gas-oil-water-hydrate flow, heat and mass transfer, flow assurance.

Abstract

This article presents the coupling of a crystallization model of gas hydrate formation to a mechanistic gas-liquid slug flow model. Crystallization of gas hydrates occurs within multiphase flow in oil and gas production operations. Mass transfer (gas absorption and convection up to the growing surface) and heat transfer (since gas hydrate formation is exothermic, thus competitive to the driving force required to hydrates to keep forming) limit crystallization under flow. The model is used to understand these competitive phenomena.

Introduction

Gas hydrates are crystals formed by the imprisonment of gas molecules inside cages made of hydrogen-bonded water molecules (Sloan and Koh, 2008). Both multiphase flow and gas hydrate formation have been widely studied due to their application in oil and gas production operations, and to this date relevant advances in modeling and experimentation have been made. However, only recently studies coupling gas hydrate formation to multiphase flow have appeared in the literature. The interest is to understand how gas consumption and heat release due to hydrate formation affect mass, momentum and energy balances of the flow (Bassani et al., 2018); and how the thermodynamic state of the mixture and the flow interfaces influence the mass transfer process in crystal growth kinetics. Furthermore, the existing flow pattern right before gas hydrate onset affects the initial size of the particles, with consequences on the slurry stability. Pipe blockage is imminent whenever the slurry becomes unstable and settles down, what might cause flow stoppage or impairment with consequential revenue losses.

This study couples a new growth model for gas hydrate formation considering the interactions between the hydrate porous structure and the gas mass transfer process in the flow, introducing it into a mechanistic slug flow model (Bassani et al., 2018).

Mathematical model

The liquid is regarded as a water-in-oil emulsion, where the gas-liquid assumes the slug flow pattern, as depicted in **Figure 1**(a). The droplet size is herein considered as being equal to the experiments, but in the future they can be properly estimated by models such as the Hinze-Brauner criterion (Brauner, 2001). Crystal nucleation occurs mainly on a droplet's surface, quickly trapping all the available water inside the porous structure of the hydrates, since those latter are hydrophilic (Hirata and Mori, 1998).

This porous structure is herein referred to as a 'sponge'. Figure 1(b) shows the path of the gas molecules up to reaching the water inside the capillaries in order to crystallize on the capillary walls. Gas solubilizes in the oil, distributes in the bulk, transfers to the outer surface of the particles and solubilizes in the water at the capillary entrance. At this point, concomitant gas diffusion through the capillary and crystallization on their walls occur. The modeling of these competitive phenomena yields the gas consumption rate per capillary $-dn_{g,i}/dt\big|_{1\ cap}$ and the evolution in time of the gas concentration in the bulk C_b:

$$-\left.\frac{dn_{g,i}}{dt}\right|_{1\ cap} = \frac{\pi r_c^{3/2}}{(1+\omega)}\sqrt{2H_w D_w k_i}\left(\frac{C_b}{H_o} - f_{eq}\right) \tag{1}$$

$$\frac{dC_b}{dt} = \underbrace{\frac{k_{g/o}A_{g/o}}{\forall_o}\left(C_{g/o} - C_b\right)}_{\text{gas absorption from the gaseous free phase by the bulk}} - \underbrace{\frac{n_p n_c}{\forall_o}\left.\frac{dn_{g,i}}{dt}\right|_{1cap}}_{\text{bulk depletion due to hydrate formation}} \tag{2}$$

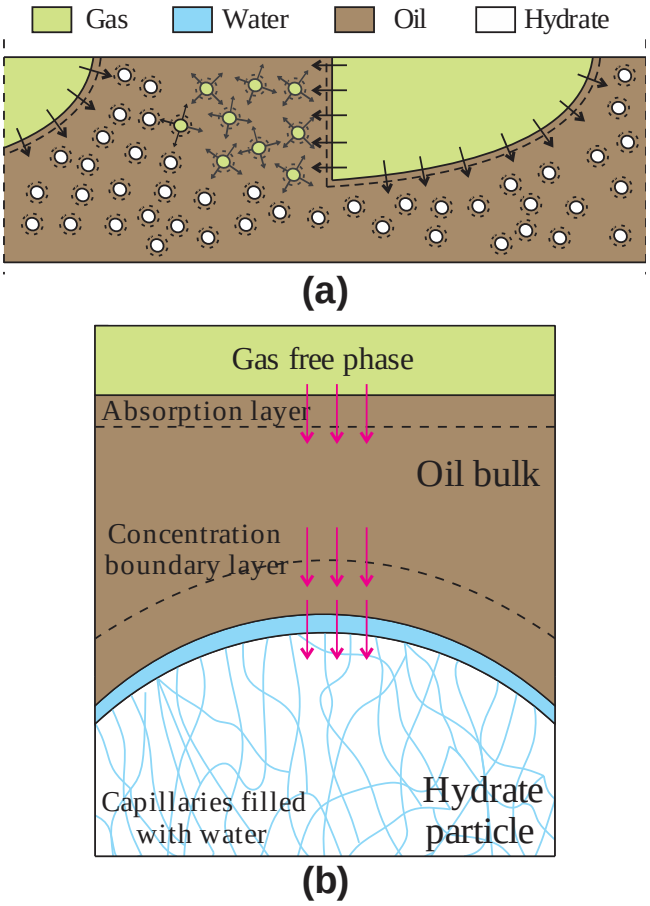

Figure 1. (a) Gas-(water-in-oil) slug flow gives rise to hydrate particles with size similar to the water droplets. (b) Gas mass transfer process up to the capillary walls where crystallization occurs.

where r_c is the capillary radius; H_w and H_o are the Henry constants of gas in water and oil, respectively (given in their solubility form, units of mol/(m^{3}Pa); Sander, 2015); D_w is the gas diffusivity in water; k_i is the constant of proportionality of the crystal integration process using a 1st order law in terms of the fugacity difference at the growing surface (related to the local concentration coming from the mass transfer process) and the three-phase gas-water-hydrate equilibrium condition (f_{eq}); $k_{g/o}$ is the absorption coefficient of gas into oil; $A_{g/o}$ is the gas-oil interfacial surface; $\forall_o$ is the oil volume; $C_{g/o}$ is the gas concentration at the gas-oil interface, considered as saturated (equilibrium at the interfaces), $C_{g/o} = H_o f_g$, where f_g is the gas fugacity at the gaseous free phase; n_p is the number of particles in the system (herein considered constant); and n_c is the number of particles per particle (which evolves in time as the capillaries fill up). Parameter ω represents the competition of (i) mass transfer between the particle and the bulk against (ii) diffusion and crystallization resistances inside the capillary:

$$\omega = \frac{n_c}{h_{m,p/b}} \frac{H_w}{H_o} \frac{r_c^{3/2}}{4r_p^2} \sqrt{\frac{2D_w k_i}{H_w}} \tag{3}$$

where $h_{m,p/b}$ is the mass transfer coefficient between the particle and the bulk (given by a Sherwood correlation for convection over spheres; Bird et al., 2002); and r_p is the particle radius (considered equal to the droplet prior to the onset of hydrate formation). The number of particles and their radius are considered constant over the process. Although 100% conversion of water does not influence the particle size noticeably (which grows at a ratio of $\rho_w/\rho_h \approx 1.09$ for methane hydrates), agglomeration can drastically change the number of particles and their average size as well. Agglomeration is neglected for the sake of simplification, but further coupling with proper population balance models must be done (Herri et al., 1999; Sampaio et al., 2017). The gas mass consumption rate due to hydrate formation comes:

$$\left.\frac{dm_g}{dt}\right|_{hyd} = n_p n_c M_g \left.\frac{dn_{g,i}}{dt}\right|_{1\,cap} \tag{4}$$

where M_g is the molar mass of the gas. This consumption rate is used to update the superficial velocity of the phases along the pipeline:

$$j_{g(n+1)} = \underbrace{j_{g(n)} \frac{Z_{(n+1)}}{Z_{(n)}} \frac{P_{(n)}}{P_{(n+1)}} \frac{T_{(n+1)}}{T_{(n)}}}_{\text{gas expansion/contraction}} + \underbrace{\frac{1}{\rho_g A} \frac{dm_g}{dt} \frac{\Delta z}{L_U}}_{\text{gas consumption term}} \tag{5}$$

$$j_{w(n+1)} = j_{w(n)} + \underbrace{\frac{\eta}{\rho_w A} \frac{M_w}{M_g} \frac{dm_g}{dt} \frac{\Delta z}{L_U}}_{\text{water consumption term}} \tag{6}$$

$$j_{h(n+1)} = j_{h(n)} + \underbrace{\frac{(\eta+1)}{\rho_h A} \frac{M_h}{M_g} \left.\frac{dm_g}{dt}\right|_{hyd} \frac{\Delta z}{L_U}}_{\text{hydrate formation term}} \tag{7}$$

where (n) and $(n+1)$ indicate the nodes of the pipeline, Z is the gas compressibility factor, P is the mixture pressure, T is the mixture temperature, M_w and M_h are the molar masses of water and hydrates, respectively, $\eta \approx 6$ is the hydration number for methane sI hydrates, and $\Delta z/L_U$ is the ratio between the nodal distance and the slug flow's unit cell length.

The lengths of the slug flow regions and their respective phase fractions are estimated through Taitel and Barnea (1990) model, coupled with correlations for the slug flow frequency (Schulkes, 2011), the unit cell translational velocity (Bendiksen, 1984) and the gas aeration in the slug body (Gomez et al., 2000). Pressure and temperature distributions along the pipeline are estimated as (Bassani et al., 2018, 2017, 2016; Taitel and Barnea, 1990):

$$P_{(n+1)} = P_{(n)} - \left[\underbrace{\frac{\tau_{LS} S_{LS}}{A} \frac{L_S}{L_U}}_{\text{friction in the slug region}} + \underbrace{\frac{\left(\overbrace{\tau_{LB} S_{LB}}^{\text{film}} + \overbrace{\tau_{GB} S_{GB}}^{\text{bubble}} + \overbrace{\tau_i S_i}^{\text{G-L interface}} \right)}{A} \frac{L_B}{L_U}}_{\text{friction in the elongated buble region}} + \underbrace{K \rho_L \frac{\left(U_{LB} - U_T \right)^2}{2 L_U}}_{\text{head loss in the elongated bubble rear}} + \underbrace{\left(\rho_L R_{LS} + \rho_G R_{GS} \right) \frac{L_S}{L_U} g \cos\gamma}_{\text{slug region weight}} + \underbrace{\left(\rho_L R_{LB} + \rho_G R_{GB} \right) \frac{L_B}{L_U} g \cos\gamma}_{\text{elongated bubble region weight}} \right] \Delta z \quad (8)$$

$$T_{(n+1)} = \frac{p}{n} + \left(T_{(n)} - \frac{p}{n} \right) \exp\left(-\frac{n}{m} \Delta z \right) \quad (9)$$

$$m = \underbrace{\rho_m c_{P,m} A L_U U_T}_{\text{sensible heat}} \quad (10)$$

$$n = q - \underbrace{\frac{\beta_G}{\rho_G} \left(\dot{m}_{GU} + \dot{m}_{Gz} \right) L_U \frac{dP}{dz}}_{\text{gas expansivity}} \quad (11)$$

$$p = q T_W + \underbrace{\Delta E_{hyd} M_G \left(-\left. \frac{dn_g}{dt} \right|_{hyd} \right)}_{\text{heat release due to gas hydrate formation}} + \underbrace{\underbrace{\tau_{LS} S_{LS} L_S U_{LS}}_{\text{slug}} + \underbrace{\tau_{LB} S_{LB} L_B U_{LB}}_{\text{film}} + \underbrace{\tau_{GB} S_{GB} L_B U_{GB}}_{\text{elongated bubble}} + \underbrace{\tau_i S_i L_B \left(U_{GB} - U_{LB} \right)}_{\text{gas-liquid interface}}}_{\text{viscous dissipation}} \quad (12)$$

$$q = \underbrace{\left(\overbrace{h_{GB} S_{GB} L_B}^{\text{elongated bubble}} + \overbrace{h_{LB} S_{LB} L_B}^{\text{film}} + \overbrace{h_{LS} S_{LS} L_S}^{\text{slug}} \right)}_{\text{heat exchange with pipeline wall}} - \underbrace{\left(\dot{m}_{Lz} c_{P,L} + \dot{m}_{Gz} c_{P,G} \right) \kappa}_{\text{heat exchange between two consecutive unit cells}} \quad (13)$$

$$\kappa = \exp\left(\frac{h_{LB} S_{LB} L_B + h_{GB} S_{GB} L_B}{\rho_{mB} c_{P,m} A J} \right) - \exp\left(-\frac{h_{LS} S_{LS} L_S}{\rho_{mS} c_{P,m} A J} \right) \quad (14)$$

where L is the length of the slug flow regions; U is the actual velocity of the phase inside each region, with related wetted surface S, shear stress τ and heat transfer coefficient h; T_W is the wall temperature; ΔE_{hyd} is the enthalpy of formation of gas hydrates; U_T is the unit cell translational velocity; and J is the mixture superficial velocity. Indexes are '*B*' for elongated bubble, '*S*' for slug, '*U*' for slug flow unit cell, '*G*' for gas phase, '*L*' for liquid phase (dispersion of water-in-oil or hydrate-in-oil) and '*i*' for gas-liquid interface. The liquid properties take the hydrate fraction after hydrate formation onset into account by assuming a homogeneous model. The slurry viscosity is the exception, computed through Krieger and Dougherty (1959).

Experiments and model validation

Validation of the slug flow model against experimental data in lab conditions was already published in previous articles (Bassani et al., 2018, 2016). The following maximum percentage deviations were found: (i) ±15% for the temperature gradient; (ii) ±20% for the pressure gradient, for the gas fraction in the elongated bubble and for the lengths of the unit cell and the elongated bubble; (iii) ±35% for the mixture heat transfer coefficient; and (iv) ±60% for the slug length.

Table 1. Characteristics of the experiments for methane hydrate formation in a flowloop following the method presented in Melchuna et al. (2016).

Fluids	Dissolved Methane / Kerdane / Deionized water
Pipeline internal diameter	10.2 mm
Flowloop extensions	30 m -4º declined section (rolled, curves of 60D) 10 m upward vertical section 8 m downward vertical section
Mixture temperature	278 K
Mixture pressure	80 bar
Mixture velocity	0.68 m/s
Water cut	32.25 %
Volume of mixture inside flowloop	10 L
Droplet diameter before hydrates onset	0.8 - 4 mm, average diameter of 2 mm (High Speed Imaging)
Crystal integration constant (Al-Otaibi, 2009)	$k_i = 8 \times 10^{-8} \ \frac{\text{mol}}{\text{m}^2 \text{sPa}}$
Absorption coefficient (Herri et al., 1999; Melchuna, 2016)	$\frac{k_{g/b} A_{g/b}}{\forall_b} = 1 \times 10^{-2} \ s^{-1}$
Kerdane properties (Total, 2015)	$H_o \approx 2.7 \times 10^{-4} \frac{mol}{m^3 Pa}$ (80 bar, 5ºC) $\rho_o \approx 815 \ \text{kg/m}^3$ $\mu_o = 2 \times 10^{-3}$ Pa.s (Newtonian behavior, measured in rheometer at 4ºC, 1 bar)
Methane hydrate properties (Jung et al., 2010; Sloan and Koh, 2008)	$\rho_h \approx 917 \ \frac{\text{kg}}{\text{m}^3}$ $\Delta E_{hyd} = 53 \times 10^3$ J/mol $M_h \approx 17.7 \times 10^{-3} \frac{\text{kg}}{\text{mol}}$; $\eta = 6$
Initial porosity and capillary radius (Klapp et al., 2010)	$\varepsilon_{\text{sup},in} = 15\%$; $r_c = 350nm$
Birth-to-death ratio of capillaries (curve fitted)	$1 - \lambda_c = 8 \times 10^{-6}$
Overall efficiency of the model (curve fitted)	$\alpha_p = 2.65 \times 10^{-3}$

The kinetic model needs curve fitting of two parameters: the birth-to-death ratio of capillaries (λ_c) and an overall efficiency of the kinetic model (α_p, which multiplies the RHS of Eq. (4)). The latter is interpreted as the amount of particles that actually interact with the system on consuming gas for crystallization. Furthermore, α_p 'corrects' any inconsistency in the order of magnitude of the closure parameters chosen from literature, since exact values of some of the micro-scale closure parameters are not available in literature. As an example, the constant of proportionality of the crystal integration process presents a range of 5 orders of magnitude in literature for methane hydrates $\left(k_i \approx 5.5 \times 10^{-12} \text{ to } 1.8 \times 10^{-7} \text{ mol}/(\text{m}^2 \cdot \text{s} \cdot \text{Pa}) \right)$; Al-Otaibi, 2009; Englezos et al., 1987; Sharma, 1996). Furthermore, parameters such as the initial surface porosity and the capillary radius were found only for permafrost hydrates (Klapp et al., 2010).

Table 1 presents the parameters used to fit the model curve against experimental data measured with the flowloop described in Melchuna et al. (2016). The main modification in the flowloop was the introduction of a sapphire window to estimate the droplet size before the onset of hydrate formation with High Speed Imaging.

Figure 2 presents the comparison of the molar amount of gas consumed in time predicted by the model with the experimental data. The model is capable of predicting the asymptote of gas consumption due to the evolution of the porosity in time, commonly called mass transfer limitation process.

Figure 3 presents photographs of the water-in-oil dispersion flow before hydrate formation and 10 s after that. The hypothesis that all droplets convert almost instantly to hydrates is valid. However, the model needs to be extended to consider agglomeration, since much larger particles then the prior droplets appear. Furthermore, the water-in-oil dispersion flow is dense, thus the bulk existence hypothesis of the model is probably not valid for the whole mixture volume. We are currently working on the experimental data and further curve fitting of the kinetic model shall be presented in literature in a near future.

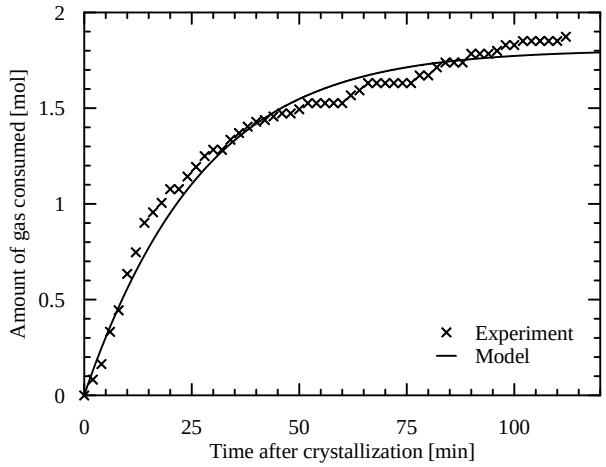

Figure 2: Model trend validation against experimental results for the molar amount of gas consumed over time.

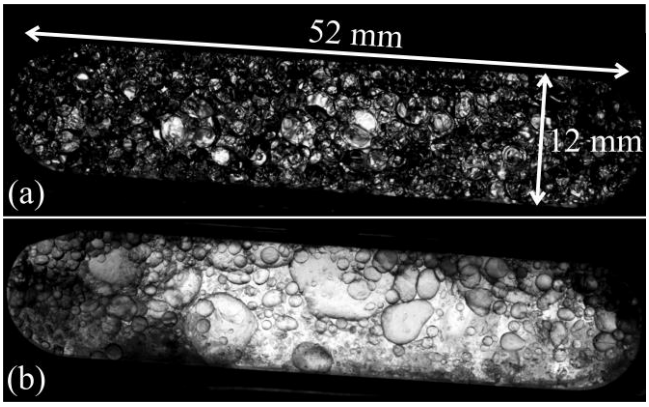

Figure 3. High Speed Imaging photos of: (a) the water-oil emulsion flow before the onset of hydrate formation and (b) 10 s after hydrates onset.

Results and discussions

The model for gas hydrate formation inside slug flow is used to understand heat and mass transfer limitations on hydrate growth kinetics.

Table **2** presents the input parameters for the model evaluation. The overall efficiency (small in the validation case, but probably higher once a free gaseous phase is introduced), was varied in order to capture different orders of magnitude of mass transfer limitation. Since the kinetic model is not yet fully validated, only trends are analyzed.

Table 2. Input parameters for model evaluation.

Pipeline length / ID / width	2 km / 26 mm / 1 mm
Pipeline inclination	Horizontal
Pipeline conductivity	30 W/(m.K)
Gas superficial velocity	1 m/s
Liquid superficial velocity	1 m/s
Water cut	30%
Fluids	CH_4 / H_2O / Kerdane
Pressure at the inlet	100 bar
Temperature at the inlet	288 K
External medium temperature	277 K
External medium heat transfer coefficient	100 W/(m^2K)

Figure 4 presents the sensitivity of the model to different overall efficiencies of the kinetic model. The dimensionless supersaturation at the capillary entrance is defined as the driving force divided by the equilibrium condition, $\bar{C}_{out,w} = \left(C_{out,w} - H_w f_{eq}\right) / H_w f_{eq}$ (Figure 4(b)). Also, since an open system was simulated (differently from the closed flowloop system used to validate the kinetic model), we adhere to the analysis of the water conversion instead of the amount of gas consumed (Figure 4(d)). The trends of Figure 4 can be split into:

(I) Heat transfer limited case (magenta line with stars): in this case, the external medium cannot absorb all the heat released due to gas hydrate formation and therefore the mixture reheats towards the equilibrium temperature, achieving a nearly constant subcooling (Figure 4(a)). This reheating causes the supersaturation in the capillaries to decrease (Figure 4(b)) due to: (i) increase in the three-phase hydrate-water-gas equilibrium fugacity related to the system temperature increase; and (ii) decrease in the solubility of gas inside water at higher temperatures (that is, lower solubilization in oil-water interface). With a shorter gas supply, the capillary filling-up rate decreases and the porosity shows a slower decrease (Figure 4(c)), and therefore the growth process lasts longer. The hydrate formation rate is nearly constant in the heat transfer limited system, and therefore the water conversion rate grows linearly (Figure 4(d)).

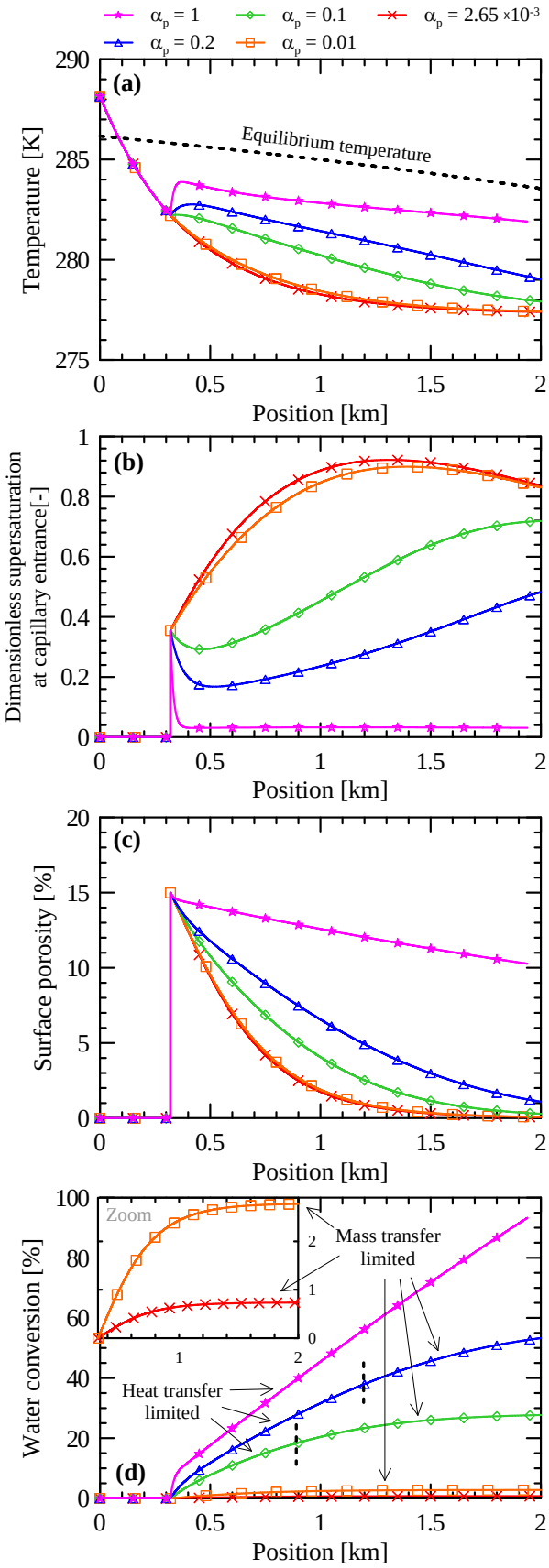

Figure 4. Evaluation for different overall efficiency of the kinetic model showing heat and mass transfer limitations. Distributions along the pipeline of: (a) mixture temperature, (b) surface porosity of the particles, (c) dimensionless supersaturation at capillary entrance, and (d) water conversion.

(II) Mass transfer limited cases (red line with crosses and orange line with squares): the heat exchange between the mixture and the outer medium is enough to dissipate all the heat released due to hydrate formation and to continue to cool the mixture down further still (Figure 4(a)). Since the driving force is kept high, a considerable supersaturation is supplied in the capillaries (Figure 4(b)) and the porous structure fills up faster (Figure 4(c)). As the porosity drops down, the gas consumption rate decreases and the water conversion presents an asymptote (zoom within Figure 4(d)).

(III) Competitive heat and mass transfer limitations (green line with diamonds and blue line with triangles): the heat exchange from the mixture to the outer medium dissipates part of the heat released due to hydrate formation, but cannot keep cooling the mixture down (Figure 4(a)). The more the mixture reheats, the lower the driving force and the lower the supersaturation in the capillary (Figure 4(b)), incurring in a lower decrease in porosity (Figure 4(c)). When the porous structure starts to fill up, the amount of hydrate formation decreases, with a consequent decrease in heat release. Therefore, the mixture starts to cool down again (Figure 4(a)), thus increasing supersaturation in the capillaries (Figure 4(b)). As a rule-of-thumb, one can say that heat transfer would mostly limit the growth process in the beginning of gas hydrate formation, where heat release is higher due to the presence of higher hydrate porosities. With time, the porous structure fills up and the process starts to be mass transfer-limited. This can be seen in the water conversion (Figure 4(d)), which presents a linear trend (heat transfer-limited, from 0.5 to ~ 1 km) that changes to a curved trend (mass transfer-limited, from ~1 to 2 km).

Conclusions

A new kinetic model for gas hydrate formation in water-in-oil dispersion flows was coupled to a slug flow mechanistic model. The kinetic model was compared to preliminary experiments of gas hydrate formation over water-in-oil dispersion flow with dissolved gas, which points to the necessity of further improvements in modeling the agglomeration process, in enhancing the knowledge of micro-scale parameters of the model (crystal integration process and porous structure). By analysis of the model trend behavior, competitive heat extraction from the pipeline and heat release due to the exothermic nature of gas hydrate formation cause a heat transfer limitation process in the crystallization. With heat transfer limitation, the hydrate structure remains ‘porous’ for a longer time due to lower supersaturations at the growing surface. Therefore, the water tends to have a higher conversion rate for the heat transfer-limited case.

Acknowledgements

The authors acknowledge the financial support of Région AURA Auvergne Rhône-Alpes through the project

COOPERA FluEnergy, the Institut Mines-Télécom, the Coordination for the Improvement of Higher Education Personnel - Brazil (CAPES) - Finance Code 001, and TE/CENPES/PETROBRAS (5850.0103370.17.9). The authors acknowledge the technical support of M.Sc. Rafael Fabrício Alves with High Speed Imaging.

References

Al-Otaibi, F.D., 2009. Kinetic studies of gas hydrate formation using in situ particles size analysis and Raman spectroscopy, PhD Thesis. University of Calgary.

Bassani, C.L., Barbuto, F.A.A., Sum, A.K., Morales, R.E.M., 2018. A three-phase solid-liquid-gas slug flow mechanistic model coupling hydrate dispersion formation with heat and mass transfer. Chem. Eng. Sci. 178, 222–237. https://doi.org/10.1016/j.ces.2017.12.034

Bassani, C.L., Pereira, F.H.G., Barbuto, F.A.A., Morales, R.E.M., 2017. Evaluation of the gas contribution to the momentum and energy balances for liquid-gas slug flows in high pressure scenarios using a mechanistic approach, in: IV Journeys in Multiphase Flows, ABCM, JEM-2017-0016, São Paulo, Brazil.

Bassani, C.L., Pereira, F.H.G., Barbuto, F.A.A., Morales, R.E.M., 2016. Modeling the scooping phenomenon for the heat transfer in liquid-gas horizontal slug flows. Appl. Therm. Eng. 98, 862–871. https://doi.org/10.1016/j.applthermaleng.2015.12.104

Bendiksen, K.H., 1984. An experimental investigation of the motion of long bubbles in inclined tubes. Int. J. Multiph. Flow 10, 467–483.

Bird, R.B., Stewart, W.E., Lightfoot, E.N., 2002. Transport Phenomena, 2nd ed, Applied Mechanics Reviews. John Wiley & Sons.

Brauner, N., 2001. The prediction of dispersed flows boundaries in liquid-liquid and gas-liquid systems. Int. J. Multiph. Flow 27, 885–910.

Englezos, P., Kalogerakis, N., Dholabhai, P.D.D., Bishnoi, P.R.R., 1987. Kinetics of formation of methane and ethane gas hydrates. Chem. Eng. Sci. 42, 2647–2658. https://doi.org/10.1016/0009-2509(87)87015-X

Gomez, L.E., Shoham, O., Taitel, Y., 2000. Prediction of slug liquid holdup: Horizontal to upward vertical flow. Int. J. Multiph. Flow 26, 517–521. https://doi.org/10.1016/S0301-9322(99)00025-7

Herri, J.M., Pic, J.S., Gruy, F., Cournil, M., 1999. Methane hydrate crystallization mechanism from in-situ particle sizing. AIChE J. 45, 590–602.

Hirata, A., Mori, Y.H., 1998. How liquids wet clathrate hydrates: some macroscopic observations. Chem. Eng. Sci. 53, 2641–2643. https://doi.org/10.1016/S0009-2509(98)00078-5

Jung, J.W., Espinoza, D.N., Santamarina, J.C., 2010. Properties and phenomena relevant to CH4-CO2 replacement in hydrate-bearing sediments. J. Geophys. Res. Solid Earth 115, B10102. https://doi.org/10.1029/2009JB000812

Klapp, S.A., Hemes, S., Klein, H., Bohrmann, G., MacDonald, I., Kuhs, W.F., 2010. Grain size measurements of natural gas hydrates. Mar. Geol. 274, 85–94. https://doi.org/10.1016/J.MARGEO.2010.03.007

Krieger, I.M., Dougherty, T.J., 1959. A mechanism for non-newtonian flow in suspensions of rigid spheres. Trans. Soc. Rheol. 3, 137–152.

Melchuna, A., Cameirao, A., Herri, J.M., Glenat, P., 2016. Topological modeling of methane hydrate crystallization from low to high water cut emulsion systems. Fluid Phase Equilib. 413, 158–169. https://doi.org/10.1016/j.fluid.2015.11.023

Melchuna, A.M., 2016. Experimental study and modeling of methane hydrates crystallization under flow from emulsions with variable fraction of water and anti-agglomerant. PhD Thesis, Mines Saint-Etienne, Saint Étienne, France.

Sampaio, T.P., Tavares, F.W., Lage, P.L.C., 2017. Non-isothermal population balance model of the formation and dissociation of gas hydrates. Chem. Eng. Sci. 163, 234–254. https://doi.org/10.1016/j.ces.2016.12.012

Sander, R., 2015. Compilation of Henry's law constants (version 4.0) for water as solvent. Atmos. Chem. Phys. 15, 4399–4981. https://doi.org/10.5194/acp-15-4399-2015

Schulkes, R., 2011. Slug frequencies revisited, in: 15th International Conference on Multiphase Production Technology. BHR Group, Cannes, France, pp. 311–325.

Sharma, S., 1996. Gas hydrate particle size measurements. University of Calgary.

Sloan, E.D., Koh, C.A., 2008. Clathrate hydrates of natural gases, 3rd ed. Taylor & Francis Group, Boca Raton, USA.

Taitel, Y., Barnea, D., 1990. A consistent approach for calculating pressure drop in inclined slug flow. Chem. Eng. Sci. 45, 1199–1206. https://doi.org/10.1016/0009-2509(90)87113-7

Total, 2015. Kerdane D 75: Safety Data Sheet.